Simultaneous detection and localization of secondary ions and electrons from single large cluster impacts

M. J. Eller,[a] S. V. Verkhoturov,[a] F. A. Fernandez-Lima,[a] J. D. DeBord,[a] E. A. Schweikert[a]* and S. Della-Negra[b]

The use of large cluster primary ions (e.g. C_{60}, Au_{400}) in secondary ion mass spectrometry has become prevalent in recent years due to their enhanced emission of secondary ions, in particular, molecular ions (MW ≤ 1500 Da). The co-emission of electrons with SIs was investigated per projectile impact. It has been found that SI and electrons yields increased with increasing projectile energy and size. The use of the emitted electrons from impacts of C_{60} for localization has been demonstrated for cholesterol deposited on a copper grid. The instrumentation, methodologies, and results from these experiments are presented. Copyright © 2012 John Wiley & Sons, Ltd.

Introduction

The scope of secondary ion mass spectrometry (SIMS) for molecular analysis has been expanded with the introduction of massive projectiles as primary ions.[1] These projectiles generate higher secondary ion (SI) yields compared to atomic or polyatomic projectiles.[2] These projectiles also exhibit significant electron emission.[3] We report here on the concurrent detection of ions and electrons from single impacts.

There are few data on electron emission from C_{60} impacts in the keV energy range. They report electron emission from Au and CsI targets 'well below the classical kinetic emission threshold'.[4,5] Further, it has been shown that electron emission increases with increasing projectile energy. Additionally, the electron emission depends on the composition, topology, and morphology of the surface. The electron emission has also been found to be independent from the type and number of co-emitted negative SIs for a range of organic, inorganic, and metallic targets.[3,6,7]

The experiments were performed in the event-by-event bombardment-detection mode, in which each projectile is separated in time and space. This mode of operation has several advantages. First, this mode of operation is performed in the super-static regime, ($<1 \times 10^9$ ions/cm^2), thus each impact probes an unperturbed surface. Second, emitted species from each impact are detected concurrently, hence enable the measurement of the electron and ion yields. The volume of emission from each projectile impact has nanometric dimensions which allows for the analysis of individual nano-objects.[8] We describe below the localization of individual impact sites with electron detection via an electron emission microscope (EEM). Further, the localization was combined with the concurrent emission of SIs for surface mapping of molecular ions.

Instrument

The instrument used in this study is a custom built SIMS instruments, equipped with a C_{60} source, EEM, and a time-of-flight mass spectrometer, ToF-MS. Specifically, the instrument has a C_{60} effusion source capable of producing C_{60} with kinetic energies from 15 up to 50 keV.[9] The mass spectrometer is a ~1-m linear ToF-MS with an eight anode microchannel plate (MCP) detector.

Instrument operation

Event-by-event ToF-SIMS performed in negative ion mode is done by analyzing the ions that are emitted from each projectile impact by linear or reflectron ToF. In this setup, the emitted electrons are collected and counted with an EEM and serve as the start for the ToF measurement. In this mode, both electrons and ions originate from a single impact site, which has nanometric dimensions.[10] Thus, the SI location on the sample is measured by the EEM. This allows for the generation of ion specific maps or density plots where the coordinates for an ion (s) of interest are plotted.

A detailed instrument electronic configuration can be found elsewhere.[11] Briefly, the EEM is equipped with a fast digital camera, MotionScope M3 (Integrated Design Tools), a monochrome 1.3 megapixel CMOS camera, which acts as the master for the time to digital converter (TDC) (CTNM4, IPN-Orsay), which operates in slave mode. Upon detection of an electron impact on the start detector, a pulse generator triggers the camera to capture the electron image. Once the camera begins to acquire the image, it triggers a second pulse generator which produces

* *Correspondence to: Emile Schweikert, Department of Chemistry, Texas A&M University, College Station, TX 77842–3012, USA.*
E-mail: schweikert@chem.tamu.edu

a *Department of Chemistry, Texas A&M University, College Station, TX, 77842-3012, USA*

b *Institut de Physique Nucléaire d'Orsay, UMR 8608, Université Paris Sud, F91406, Orsay Cedex, France*

a pulse which is accepted by a coincidence module (Model 465, LeCroy) with the initial start signal. If both signals (pulser and initial start signal) are present, the coincidence module outputs a signal to start the TDC. This setup ensures absolute synchronization between the camera and TDC as well as eliminating any electronic jitter due to small changes in camera initiation time.

Mapping

An EEM is used to localize each projectile impact. The EEM is comprised of five einzel lenses and a position-sensitive detector (PSD). A description of the operation of the lens system follows. Lens I forms the first intermediate image of the electrons in the deflection center of the magnetic prism. Lens II accepts the image and forms a second intermediate image. The rationale for forming the image in the center of the magnetic prism is to eliminate the second-order angular aberration and first-order transverse chromatic aberration. The second intermediate image is accepted by three consecutive lenses which form the magnified image ($\leq 1000\times$ magnification) on the surface of the start detector (MCP, Photonis).

The PSD is comprised of a pair of MCPs in the chevron configuration, a phosphor screen attached to a fiber-optic plate, a sealed transition fiber-optic rod, and a fast digital camera. The aluminized phosphor screen, P43, with measured decay time of ~100 μs, is attached to a fiber optic plate and is coated with a 500-Å-thick Al layer. The phosphor screen and sealed fiber optic rod are assembled on a flange for optical imaging outside of the vacuum chamber (Beam Imaging Solutions). The fast digital camera is equipped with a high-precision (1:1) optical lens (Schneider Optics) and can record at >500 frames per second.

Each projectile impact is localized using the image of simultaneously emitted/detected electrons. Each electron image is detected by the PSD and collected by the camera. Collected images are stored sequentially on a PC in the form of an audio video interleave, avi, file. This avi file is investigated one frame at a time using image recognition software described elsewhere.[11] Briefly, coordinates were obtained for each detected electron, if a frame showed at least five electrons, a provisional center of mass was computed from the emitted electrons. A software collimation was then used to remove electrons dispersed from the initial center of mass. The software collimation is an iterative process in which an initial region of interest (ROI) is placed 200 pixels from the center of mass, any electrons detected outside of this area are removed. After the electrons outside the ROI are removed, a center of mass is recalculated using the remaining electrons. A second collimation is performed with the ROI placed 100 pixels from the second center of mass. Electrons outside of the ROI are removed, and if after this final collimation ≥ 4 electrons remain within the ROI, a new center of mass is calculated with the remaining electrons. The coordinates of the center of mass calculation were used to assign the site of a C_{60} projectile impact. By removing dispersed electrons, a reduction in the error of localization was observed which is further discussed in the results section.

The SIs are detected concurrently with the electrons via a two lens system. Lens I forms the first intermediate image in the deflection center of the magnetic prism. The weak field of the magnetic prism deflects the secondary electrons but does not affect the trajectory of the SIs. The intermediate image of SIs is accepted by a second lens, which is used for correcting the angle of the ions (non-imaging mode). The ions pass the SI optics and the ToF region and are detected by the 8 anode MCP detector (Photonis).

Results

The electron probability distributions follow a Poisson distribution (see example in Fig. 1 which corresponds to data shown in Figs. 2b and 3).[12] From these distributions, the electron yield, average number of detected electrons per projectile impact, can be calculated. For example, 30-keV and 50-keV C_{60} impacts on neat glycine and cholesterol targets have electron yields of ~4. Higher electron yields are measured for Au_{400} impacts on CsI and biological samples (for example, Au_{400} at 320 keV on glycine has an electron yield of 6.4).[9]

Localization

As noted earlier, we limit localization to impacts from which at least five electrons were emitted/detected and where, additionally, at least four electrons remain after software collimation. The error of this localization calculation will define the effective probing diameter of the projectile impact. To calculate the error in localization, the equation below was used.[13] Where Δx is the error in localization, S_d is the standard deviation of the spread of the electrons, and N is the number of electrons used for localization.

$$< (\Delta x)^2 > = \frac{S_d{}^2}{N}.$$

The percent of impacts from which an impact site could be determined with the instrumental and software boundaries noted above is ~10% for 50-keV C_{60} impacts on cholesterol. Most of the non-localized impacts were from events where less than five electrons were detected (~50% of all impacts).

The error in localization was tested on a model target in which cholesterol was vapor deposited onto a 500 line per inch Cu grid (Precision Eforming). The 500 line per inch Cu grid dimensions are 50.8-μm wire center to center with a wire thickness of 11.4 μm. After vapor depositing cholesterol, the wire width was measured at ~15.7 μm by SEM (figure 2a).

The cholesterol sample was investigated with C_{60} at 50-keV total impact energy. The error in localization, Δx, without software collimation was determined to be 1.90 μm with a corresponding S_d of 5.1 μm. The preceding data are mean values from a set of individual
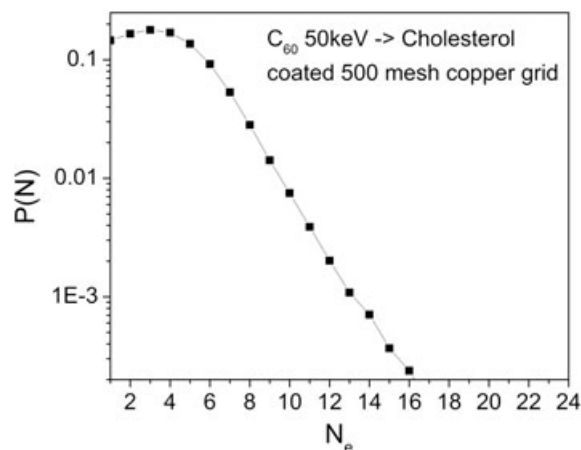
Figure 1. Measured electron distribution from C_{60} impacts at 50 keV on a cholesterol target.
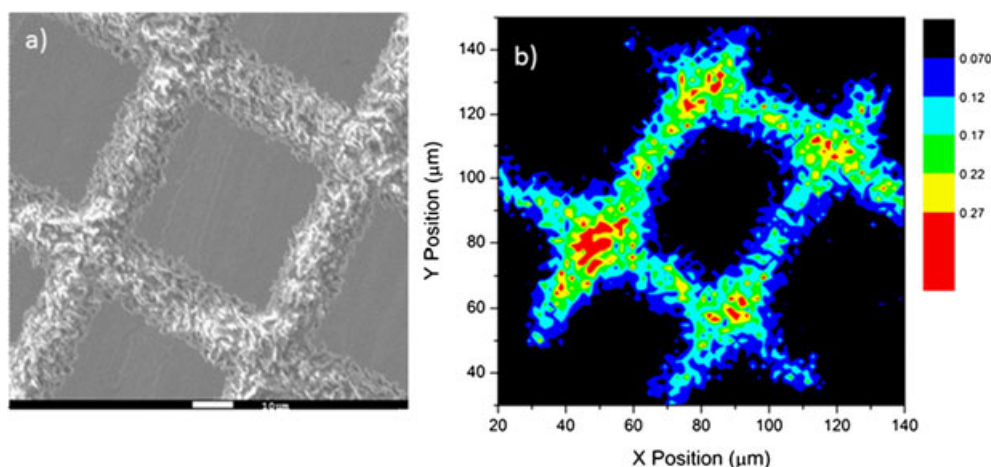
Figure 2. (a) SEM image of cholesterol coated 500 line per inch copper grid. (b) Total ion density plot of cholesterol coated 500 line per inch Cu grid.
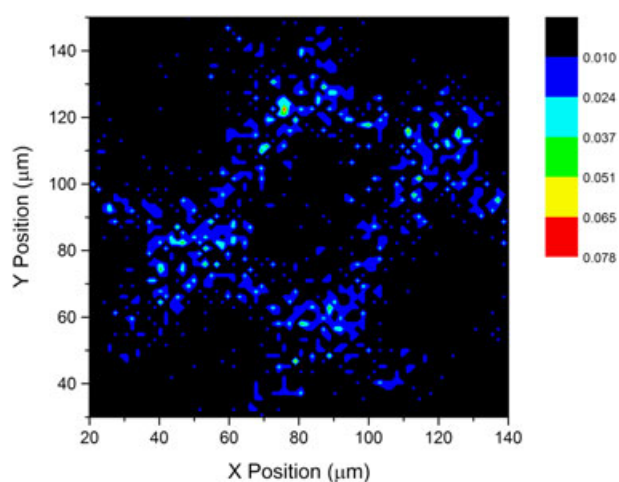
Figure 3. Ion selected density plot for the [cholesterol-H]⁻ ion from cholesterol coated 500 line per inch copper grid.

impacts (~80 k) where $N \geq 5$. After software collimation (selection of events where $N \geq 4$ in the ROI), we obtain a mean Δx of 600 nm (from ~30 k impacts) with a S_d of 1.4 µm. This Δx was obtained with a low magnification of ~150x. A total ion density plot corresponding to Δx of 600 nm is presented in Fig. 2b. The lack of definition around the edges is attributed to electron scattering and/or local electric field distortion. In this figure, the map of impacts are averaged over a 4×4 pixel area, (~500×500nm). An ion-selected density plot can be generated by selecting the impacts in which an ion(s) of interest was detected, in Fig. 3, an ion-selected density plot is presented corresponding to impacts where m/z 385, [cholesterol-H]⁻, was detected. Both density plots, total ion, and [cholesterol-H] ⁻, correspond well with the SEM image obtained.

Conclusion

We have shown the ability to localize molecular ions with individual impacts of C_{60} at 50 keV, specifically the de-protonated molecular ion of cholesterol. The measurement was obtained with the EEM at 150× magnification corresponding to a mean error in localization of 600 nm, with boundaries set in the electron detection and software collimation. Prospects for enhanced accuracy and precision with C_{60}^{n+} are feasible by increasing the magnification of the EEM. A magnification of 400× has been demonstrated earlier.[3] Clearly, increased SI and electron yields from higher impact energy C_{60} (e.g. C_{60}^{3+}) will lead to improved molecular mapping performance. The latter will be still further enhanced with the use of Au_{400}.[14,15] The significantly higher electron emission 320-keV Au_{400} versus 50-keV C_{60} and the abundant analyte specific ion yields augur well for molecular mapping beyond the performance reported here.

References

[1] N. Winograd, B. J. Garrison, *Ann. Rev. Phys. Chem.*, **2010**, *61*, 305.
[2] X. A. Conlan, J. C. Vickerman, J. S. Fletcher, N. P. Lockyer, *J. Phys. Chem. C* **2010**, *114*, 5468.
[3] S. V. Verkhoturov, M. J. Eller, R. D. Rickman, S. Della-Negra, E. A. Schweikert, *J. Phys. Chem. C* **2010**, *114*, 5637.
[4] F. Aumayr, G. Betz, T. D. Mark, P. Scheier, H. P. Winter, *Int. J. Mass Spectrom.* **1998**, *174*, 317.
[5] A. Brunelle, P. Chaurand, S. DellaNegra, Y. LeBeyec, E. Parilis, *Rapid Commun. Mass Spectrom.* **1997**, *11*, 353.
[6] S. V. Verkhoturov, M. J. Eller, S. Della-Negra, R. D. Rickman, J. E. Locklear, E. A. Schweikert, *Surf. Interface Anal.* **2011**, *43*, 49.
[7] M. J. Eller, S. V. Verkhoturov, S. Della-Negra, E. A. Schweikert, *J. Phys. Chem. C* **2010**, *114*, 17191.
[8] V. T. Pinnick, S. V. Verkhoturov, L. Kaledin, Y. Bisrat, E. A. Schweikert, *Anal. Chem.* **2009**, *81*, 7527.
[9] F. A. Fernandez-Lima, M. J. Eller, J. D. DeBord, S. V. Verkhoturov, S. Della-Negra, E. A. Schweikert, *Nucl. Instrum. Methods Phys. Res., Sect. B*, DOI: 10.1016/j.nimb.2011.07.092
[10] Z. Li, S. V. Verkhoturov, E. A. Schweikert, *Anal. Chem.* **2006**, *78*, 7410.
[11] M. J. Eller, S. V. Verkhoturov, S. Della-Negra, R. D. Rickman, E. A. Schweikert, *Surf. Interface Anal.* **2011**, *43*, 484.
[12] F. A. Fernandez-Lima, M. J. Eller, S. V. Verkhoturov, S. Della-Negra, E. A. Schweikert, *J.Phys. Chem. Lett.* **2010**, *1*, 3510.
[13] W. W. Webb, R. E. Thompson, D. R. Larson, *Biophys. J.* **2002**, *82*, 2775.
[14] J. D. DeBord, F. A. Fernandez-Lima, S. V. Verkhoturov, S. Della-Negra, E. A. Schweikert, These Proceedings.
[15] F. A. Fernandez-Lima, J. Post, J. D. DeBord, M. J. Eller, S. V. Verkhoturov, S. Della-Negra, A. S. Woods, E. A. Schweikert, *Anal. Chem.* **2011**, *83*, 8448.